Quantitative analysis and modeling of katanin function in flagellar length control

Elisa Kannegaard[a], E. Hesper Rego[b,c], Sebastian Schuck[a,*], Jessica L. Feldman[a,†], and Wallace F. Marshall[a,b,c]

[a]Department of Biochemistry and Biophysics and [b]Graduate Group in Biophysics, University of California, San Francisco, San Francisco, CA 94158; [c]Physiology Course, Marine Biological Laboratory, Woods Hole, MA 02543

ABSTRACT **Flagellar length control in *Chlamydomonas reinhardtii* provides a simple model system in which to investigate the general question of how cells regulate organelle size. Previous work demonstrated that *Chlamydomonas* cytoplasm contains a pool of flagellar precursor proteins sufficient to assemble a half-length flagellum and that assembly of full-length flagella requires synthesis of additional precursors to augment the preexisting pool. The regulatory systems that control the synthesis and regeneration of this pool are not known, although transcriptional regulation clearly plays a role. We used quantitative analysis of length distributions to identify candidate genes controlling pool regeneration and found that a mutation in the p80 regulatory subunit of katanin, encoded by the PF15 gene in *Chlamydomonas*, alters flagellar length by changing the kinetics of precursor pool utilization. This finding suggests a model in which flagella compete with cytoplasmic microtubules for a fixed pool of tubulin, with katanin-mediated severing allowing easier access to this pool during flagellar assembly. We tested this model using a stochastic simulation that confirms that cytoplasmic microtubules can compete with flagella for a limited tubulin pool, showing that alteration of cytoplasmic microtubule severing could be sufficient to explain the effect of the *pf15* mutations on flagellar length.**

Monitoring Editor
Alex Mogilner
University of California, Davis

Received: Jun 16, 2014
Revised: Jul 30, 2014
Accepted: Aug 7, 2014

INTRODUCTION

Regulation of organelle size is a critical aspect of the determination of cell architecture, but the mechanisms that determine organelle size are largely unknown (Chan and Marshall, 2010; Levy and Heald, 2012). Control of organelle size involves regulation of two separate steps: the synthesis of organelle precursor molecules, and the assembly of these precursors into the final structure. Size control by limiting the quantity of organelle precursor has been clearly demonstrated for centrosomes (Decker *et al.*, 2011) and has emerged as a potentially general scheme for organelle size determination (Goehring and Hyman, 2012). In cases in which organelle size is controlled by limiting quantities of precursors, the key question becomes what pathways exist to regulate the size of the precursor pool.

One tractable model system in which to study the interplay between precursor synthesis and assembly is the flagellum of the green alga *Chlamydomonas reinhardtii*. In this organism, flagella can be detached by pH shock and induced to rapidly regenerate, during which time genes encoding flagellar proteins are synchronously up-regulated (Keller *et al.*, 1984; Lefebvre and Rosenbaum, 1986; Stolc *et al.*, 2005). If new protein synthesis is blocked, flagella start regeneration with normal kinetics but cease growth prematurely and reach a shorter final length (Rosenbaum *et al.*, 1969; Lefebvre *et al.*, 1978), demonstrating that a preexisting pool exists that is sufficient to drive partial flagellar assembly but is insufficient to grow a full-length flagellum.

The existence of a limiting pool of precursor suggests that the size of this pool should play a role in determining the length of the flagella. In cells with increased numbers of flagella, the average

This article was published online ahead of print in MBoC in Press (http://www.molbiolcell.org/cgi/doi/10.1091/mbc.E14-06-1116) on August 20, 2014.

Present addresses: *Zentrum für Molekulare Biologie der Universität Heidelberg, D-69120 Heidelberg, Germany; †Department of Biology, Stanford University, Palo Alto, CA 94305.

Address correspondence to: W. F. Marshall (wallace.marshall@ucsf.edu).

Abbreviations used: CTAB, cetyl trimethyl ammonium bromide; DIC, differential interference contrast; GDP, guanosine diphosphate; GTP, guanosine triphosphate; IFT, intraflagellar transport; LF, long flagella; PBS, phosphate-buffered saline; PF, paralyzed flagella; RESDA, restriction enzyme site–directed amplification; RNAi, RNA interference; RSP3, radial spoke protein 3; SFH, short flagella; TAP, tris acetate phosphate.

flagellar length is decreased (Marshall *et al.*, 2005), again suggesting that the flagella share a pool of precursor proteins whose size affects the steady-state length. In the most idealized limiting precursor model, in which 100% of the precursor is consumed in the assembly process, the average size should scale as 1/*n*, where *n* is the number of copies of the organelle. This is true for centrosomes (Decker *et al.*, 2011) but not for flagella (Kuchka and Jarvik, 1982; Marshall *et al.*, 2005); however, such idealized scaling is predicted only if the pool is completely consumed, and if the pool is in a dynamic equilibrium with the organelles, the dependence on *n* is expected to be less steep than 1/*n* (Marshall *et al.*, 2005). Overall we expect there to be a strong link between pool size and flagellar length, making it essential to understand the mechanisms that regulate pool size. One barrier to understanding pool size control is that we do not know which flagellar protein or proteins are limiting for flagellar growth. Because the structural core of the flagellum is composed of tubulin, we imagine that tubulin may be the limiting precursor, but this has not yet been demonstrated. If tubulin was the limiting precursor, then the protein machinery that regulates microtubule dynamics would be predicted to influence the effective pool size regulating flagellar length.

Better understanding of pool regeneration would provide an important missing link in our understanding of flagellar length control. One length control model that has been proposed is a balance-point mechanism in which length is set by the dynamic balance between turnover of axonemal microtubules and the inherently length-dependent transport of new tubulin to the tip by the intraflagellar transport system (Marshall and Rosenbaum, 2001; Marshall *et al.*, 2005; Wemmer and Marshall, 2007; Engel *et al.*, 2009). This model is supported by the fact that tubulin has been shown to be a cargo that is carried by the intraflagellar transport (IFT) system (Qin *et al.*, 2004; Hao *et al.*, 2011; Bhogaraju *et al.*, 2013). An alternative model is that a length sensor is used to construct a feedback control system in which the flagellum grows until it reaches the correct length and then stops due to changes in activity of a length-responsive signaling pathway (Wilson *et al.*, 2008). Such a feedback mechanism is supported by the fact that IFT particle injection into flagella is a function of length (Ludington *et al.*, 2013) and that loading of some cargo proteins onto the IFT system may also be a function of length (Wren *et al.*, 2013). Current models focus almost entirely on IFT itself and do not address the mechanisms that might regulate the size of the precursor pool.

In this study we used a set of short-flagella mutants in the unicellular green alga *C. reinhardtii* obtained in a previous screen for phototaxis-defective mutants (Feldman *et al.*, 2007) as a starting point to search for mutations affecting precursor pool synthesis. This organism has long been a favored system for genetic studies of flagellar biology due to its ease of culture and tractable yeast-like haploid genetics. *Chlamydomonas* cells possess two flagella, each typically 10–12 µm in length. *Chlamydomonas* genetic analyses have yielded a handful of genes that alter flagellar length, including three *SHF* genes, whose mutants cause short flagella (Kuchka and Jarvik, 1987), and four *LF* genes, whose mutants cause atypically long flagella but can also, paradoxically, cause cells to lack flagella, depending on the allele (McVittie, 1972; Barsel *et al.*, 1988; Asleson and Lefebvre, 1998). Starting with a quantitative analysis of flagellar length distributions to identify a candidate mutant with defective pool regeneration, we identified a mutation in the p80 subunit of the microtubule-severing enzyme katanin. We found that katanin mutants impaired the mobilization of the effective cytoplasmic precursor pool during flagellar regeneration, suggesting that katanin-mediated severing of cytoplasmic microtubules might make tubulin available for flagellar assembly. A simple computational model of microtubule dynamics coupled with flagellar length control confirmed that reduced katanin activity could lead to shorter flagella due to impaired mobilization of the total tubulin pool.

RESULTS

Identifying short-flagella mutants with slowed regeneration kinetics

To identify genes regulating pool synthesis, we must first have an understanding of what phenotype we should expect to observe if such genes are mutated. When flagella are severed from wild-type *Chlamydomonas* cells after pH shock, they grow back to full length in <2 h. The regeneration kinetics is biphasic, with flagella growing rapidly to approximately half-length, followed by a period of gradually slowing growth during which flagella asymptotically approach the final steady-state length (Lefebvre *et al.*, 1978). If new protein synthesis is inhibited before flagellar severing, the new flagella that regenerate can grow back only to roughly half-length, but their initial growth rate is very close to the initial rate of rapid growth in untreated cells (Lefebvre *et al.*, 1978). Thus it is the second, slower phase of growth that is affected when protein synthesis is inhibited. We hypothesized, therefore, that mutants with defects in the induction of cytoplasmic precursor pool synthesis during flagellar regeneration would be recognizable by a much slower secondary growth phase compared with wild-type cells while retaining approximately normal rates of initial rapid growth.

Direct measurement of flagellar regeneration kinetics is time-consuming and difficult to perform in parallel for large numbers of mutants, so we first asked whether there is a simpler criterion that could be more rapidly assayed as a primary screen, to be then followed by direct measurement of regeneration kinetics. The relation of growth kinetics to the length distribution of linear structures has been formalized in the population-balance method, previously developed by Aizawa and colleagues for calculating growth kinetics of the bacterial flagellar hook from the distribution of hook lengths (Koroyasu *et al.*, 1998). The principle of this method is that for a structure that undergoes monotonic growth, the fraction of such structures found within a given range of lengths in an asynchronous population is directly related to the growth rate over that size range. The faster the object is growing when at a particular size, the less frequent will be objects of that size when a population of objects is observed. For example, in a wild-type cell in which flagella grow rapidly to their final length and then remain there for a long time, few cells will have short flagella because any given cell will not spend a long period of time with short flagella, because they are rapidly growing. Therefore, in an asynchronous population, the distribution will be sharply peaked around the final steady-state length. For a hypothetical mutant defective in pool regeneration, it would not spend much time with very short lengths, since the rapid early growth phase does not involve pool regeneration. Thus the length distribution should not contain many individuals with less than half of the normal length. However, slow regeneration of the pool would mean that cells would spend more time with flagella at intermediate lengths between half-length and wild-type length, so we expect the overall distribution of lengths in a population of asynchronously dividing cells to be unusually broad and stretch between half-length and full length, with an average length that is shorter than wild type.

Although three short-flagella (*shf*) mutants have already been identified, they are difficult to clone because their mutations are not sequence tagged. We therefore screened a collection of 20 insertional short-flagella mutants that we had previously identified in

Strain	<*L*> (μm)	σ (μm)	Skew	Kurtosis	*n*
cc-125	11.0	1.1	0.06	0.43	166
shf1-253	5.2	0.3	–1.38	0.42	60
shf3-1851	10.4	0.2	–0.35	–0.26	60
pf14	2.8	1.7	1.02	1.23	21
pf15a	6.1	3.5	0.61	–0.66	153
pf18	4.2	3.0	1.53	1.37	62
pf19	1.9	1.0	1.07	0.14	90
pf20	6.1	4.3	0.34	–1.48	54
pf26	11.7	3.4	1.71	2.21	20
802 I	3.1	2.0	2.15*	5.28**	114
267 I	2.7	2.0	1.70*	2.74**	110
6648 I	2.5	2.0	2.01*	4.97**	49
6773 I	2.2	1.1	1.25*	1.82**	50
5834 I	1.9	1.5	2.01*	5.16**	110
5840 I	1.8	2.2	2.29*	4.98**	39
5836 I	0.7	0.3	1.74*	3.67**	60
9111 II	10.5	1.6	–0.88*	0.49	109
7107 II	10.2	3.2	–1.23*	2.68**	130
9484 II	10.0	1.4	–0.12	0.19	108
6894 II	9.8	1.6	–0.94*	1.72**	110
8488 II	9.4	2.7	–0.81*	0.71	110
8333 II	9.4	2.1	–0.94*	0.74	114
6444 II	9.2	3.5	–1.26*	0.80	112
8796 II	9.1	3.5	–1.48*	1.22**	83
784 III	6.8	4.0	–0.09	–1.42**	168
4580 III	5.9	3.0	–0.28	–1.36**	170
1464 III	5.1	3.3	0.74*	–0.81**	199
5899 III	5.0	3.7	0.49*	–1.05**	112
3584 III	4.7	3.7	0.43*	–1.46**	170

Roman numerals indicate the assigned length distribution class for insertional mutants.
*Significant deviation from a normal distribution, defined as a skewness statistic with absolute value greater than twice the SE of skew.
**Significant deviation from a normal distribution, defined as a kurtosis statistic with absolute value greater than twice the SE of kurtosis.

TABLE 1: Flagellar length distribution in short-flagella mutants.

a screen of 10,000 random insertional lines using a phototaxis assay (Feldman *et al.*, 2007). We analyzed the length distributions of all 20 insertional *shf* mutants, with results listed in Table 1. Although different mutants show a range of different length distributions, analysis of the shape of the length distribution, as judged by skew and kurtosis, allowed us to define three categories: class I, positive kurtosis, positive skew; class II, positive kurtosis, negative skew; and class III, negative kurtosis. The first two classes have a sharply peaked distribution that is of a shorter mean length than wild type, but because the distributions are peaked around a single value, these mutations appear to retain an effective length control system. We note that although some of these show a statistically significant positive skew, this is likely to be a byproduct of the fact that flagellar lengths cannot be negative, hence length distributions whose mean is less than the SD will produce truncated distributions and yield a positive skew when fit with a Gaussian. We focused our analysis on class III, as the negative kurtosis (flat distribution) matched our expectations for mutants with impaired pool regeneration. Class III comprised five mutants, whose length distributions are plotted in Figure 1. As can be seen, in comparison to wild type, all of these mutants show a broader distribution of lengths and decreased average length.

We next examined flagellar regeneration kinetics directly in this subclass of short-flagella mutants (Figure 2A). In all five of the candidate mutants, the regeneration curves plateau abruptly at a short length relative to wild type and in this sense are reminiscent of wild-type cells treated with protein synthesis inhibitors. Such might be the expected result for a mutant with defects in pool regeneration. However, the initial growth rate is slightly reduced compared with wild-type cells. This could indicate some pool-independent effect of the mutation, or it could indicate the presence of a reduced pool from the very beginning of the time course, unlike in wild-type cells, where the pool starts out at full capacity.

By plotting length versus time normalized to predeflagellation length, we found that four of the five mutants regenerated to half of their steady-state length within ~40 min, whereas mutant 784 had reached only one-fourth of its predeflagellation length by 100 min (Figure 2B). This suggested a severe defect in flagellar regeneration rates even at short lengths for that mutant, which does not appear to be consistent with a primary defect in pool synthesis or length regulation per se but instead may represent a more fundamental failure in one of the many necessary steps of flagellar assembly. Therefore this mutant was excluded from further analysis.

Impaired recovery of flagellar precursor pool in *shf* mutants

Slower regeneration kinetics could indicate a reduced precursor pool size but could also be caused by many other types of defects, such as reduced intraflagellar transport. Thus we next sought to measure pool regeneration in the four remaining candidate mutants. The length-limiting protein component of the flagellum is not known, and therefore it is not possible to measure the regeneration of the relevant precursor protein by direct protein analysis. However, the regeneration kinetics of the functional precursor pool can be indirectly assessed using an elegant method developed by Lefebvre and Rosenbaum (Lefebvre *et al.*, 1978), which entails performing two sequential deflagellations. In this procedure (Figure 2C), flagella are detached by pH shock and allowed to regenerate. Aliquots of cells with actively regenerating flagella are removed from the culture and subjected to a second pH shock, this time in the presence of cycloheximide, at a series of time intervals. These samples are then allowed to fully regenerate after the second shock. Because regeneration during the second shock depends on whatever precursor pool was present before the second shock was initiated (since further protein synthesis was inhibited at the same time that the second shock was performed), a plot of the final length versus the time at which the second shock was performed yields a plot of the effective pool size as a function of time. Analysis of pool dynamics using this dual-shock assay in wild-type cells showed that the pool of flagellar precursors is depleted during the first 40 min of regeneration and then begins to accumulate again (Lefebvre *et al.*, 1978).

When we applied this dual-shock measurement method to our mutants, we found that all four of the class III mutants analyzed showed pool depletion by $t = 40$ min, just as was seen in wild type, but then failed to recover the pool size back to the initial level (Figure 2D). Thus all four class III mutants tested showed an apparent effect on the regeneration of the effective precursor pool in comparison to wild-type cells. We emphasize that this measurement is not a direct

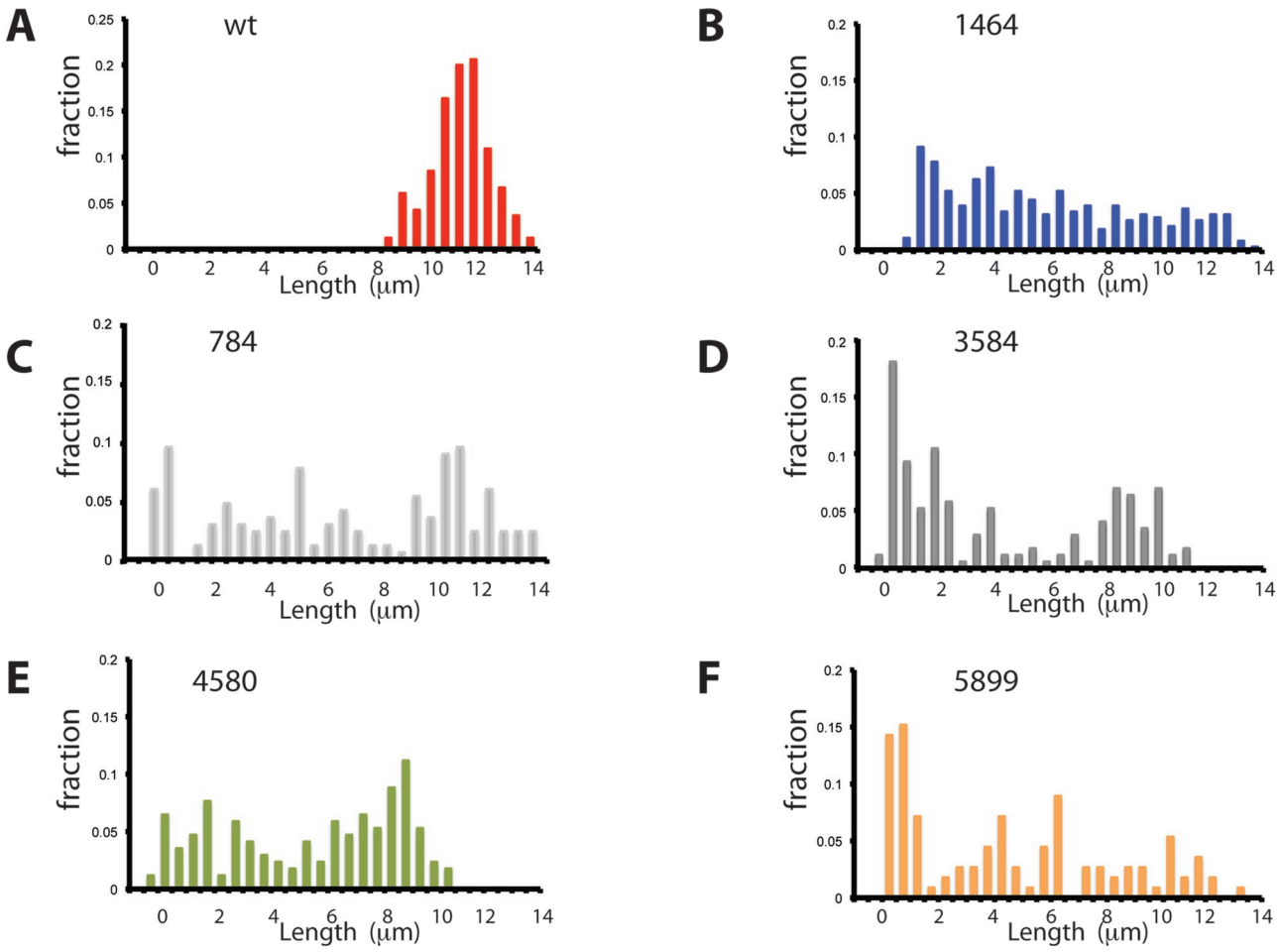

FIGURE 1: Length distribution of the class III short flagella mutants, with wild type for comparison. (A) Wild-type strain cc-124, $n = 165$ flagella measured. (B) Mutant 1464, $n = 385$. (C) Mutant 784, $n = 168$. (D) Mutant 3584, $n = 170$. (E) Mutant 4580, $n = 170$. (F) Mutant 5899, $n = 112$.

measurement of any particular protein component of the flagellum but instead is a functional measurement of the effective pool size in terms of the flagellar length that can be grown with a particular quantity of precursor.

Gene induction during flagellar assembly

Given the foregoing results, it appears that the class III mutants have a defect in regeneration of the flagellar precursor pool. The precursor pool is known to be under transcriptional control, such that during the process of regeneration, expression of flagellar genes is dramatically up-regulated (Lefebvre and Rosenbaum, 1986; Stolc *et al.*, 2005). Because a failure to induce flagellar gene expression would prevent regeneration of a precursor pool, one obvious reason for the failure to regenerate the pool in the class III mutants would be that perhaps the genes defective in these mutants are part of the pathway controlling transcription of flagellar protein–specific genes. None of the components of this pathway was known, so we were extremely interested in determining whether the class III mutants might reveal genes that regulate flagellar precursor protein–encoding genes. To do this, we tested whether the *shf* mutants in our collection were capable of proper gene induction, using quantitative reverse transcription PCR using the radial spoke protein 3 (RSP3) gene as a representative flagellar gene and the RBCS2B gene, which encodes a subunit of the abundant photosynthesis enzyme ribulose-1,5-bisphosphate carboxylase oxygenase, commonly known as RuBisCo, as a control "housekeeping" gene for normalizing expression levels.

We then examined transcriptional induction of RSP3 in our collection of mutants, as well as in several known short-flagella mutants (*shf*) and paralyzed-flagella mutants (*pf*) for comparison. We expected to find a defect in class III mutants, which showed a defect in pool regeneration as assessed in Figure 2D. Because peak induction of most flagellar genes occurs 30 min after deflagellation (Stolc *et al.*, 2005), we selected this time point for comparison of induction across strains. Figure 2, E and F, depicts the results of this analysis, which revealed extensive variation between mutant lines. The *shf3* strain and mutants 802 and 7107 had significantly higher RSP3 expression than the wild-type strain, and the strains *pf18* and *shf1* and mutants 784, 5836, and 5840 had significantly lower expression than the wild-type strain. Of interest, *shf2* mutants showed virtually no induction of flagellar genes, raising the interesting possibility that the SHF2 gene (Kuchka and Jarvik, 1987), whose product is unknown, might be involved in the transcriptional control circuit regulating flagellar gene expression. Of the low inducers, all but strain 784 were found to have significant numbers of flagella-less (bld) cells.

Surprisingly, of the class III mutants, only mutant 784 showed decreased induction of RSP3. This mutant had already been

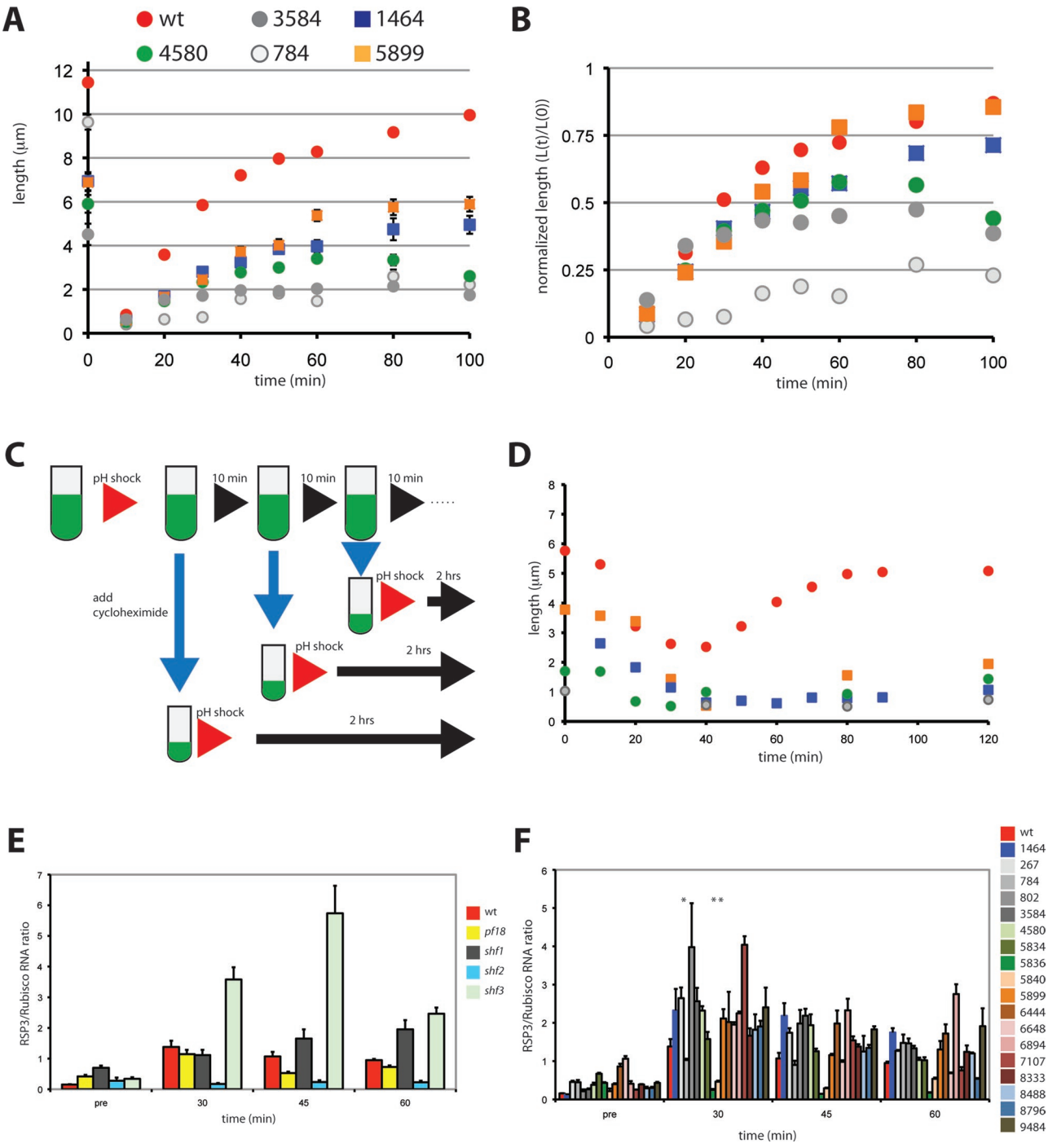

FIGURE 2: Identifying a short-flagella mutant with impaired precursor pool regeneration kinetics but normal transcriptional induction. (A) Regeneration kinetics in class III short-flagella mutants. Graph shows flagellar length vs. time after pH shock. Time 0 indicates length before pH shock. Error bars indicate SEM. Error bars smaller than the radius of the data-point marker are not visible. All data points are based on measurement of flagella from 60 cells. (B) Length vs. time after deflagellation normalized to predeflagellation length; red circles, wild type; orange squares, mutant 5899; blue squares, mutant 1464; green circles, mutant 4580; gray circles, mutant 3584; white circles, mutant 784. (C) Assay for flagellar pool regeneration as described in Lefebvre *et al.* (1978). Initial culture is subjected to pH shock (red arrow) and allowed to recover. At 10-min intervals, aliquots are removed, cycloheximide is added to the aliquot (vertical blue arrows), and then it is subjected to a second pH shock. Aliquots after the second aliquot are incubated for 2 h to reach steady-state length. (D) Result of pool regeneration assay. Time indicates the time at which the second pH shock was performed relative to when the initial pH shock was performed, that is, the time during which the cells were regenerating their pool before inhibition of protein synthesis. Length indicates the final steady-state length reached after regenerating from the second pH shock and is an indicator of the size of the protein pool at the time of cycloheximide addition; red circles, wild type; orange squares, mutant 5899; blue squares, mutant 1464; green circles, mutant 4580; gray circles, mutant 3584. (E) Induction of flagella-specific gene expression during regeneration in

excluded from having an effect only on precursor synthesis because it showed slow regeneration at all stages of regeneration (see prior discussion). In three of the four class III mutants with partial or complete loss of pool regeneration (mutants 1464, 3584, and 4580), we found that expression of RSP3 was induced at levels similar to or even greater than wild type (Figure 2F). However, the kinetics of expression were different; these three strains had significantly higher expression than the wild-type strain at 45 min postdeflagellation, although expression levels equalized by the 60-min time point. These three mutations thus result in impaired pool regeneration without an obvious reduction in transcription, suggesting that their defect in regenerating an effective precursor pool results from a posttranscriptional role in pool production or regulation. We therefore next attempted to identify the genes involved in order to learn more about the nature of the precursor pool.

Mapping and identification of katanin p80 mutation in shf strain 1464

To determine the regions flanking the inserted sequence in our collection of insertional mutants, we used restriction enzyme site-directed amplification PCR (RESDA-PCR; Gonzalez-Ballester *et al.*, 2005). Our initial RESDA-PCR results identified flanking sequence in four mutants: 1464, 3584, 4580, and 9111. However, only in line 1464 did the insertion occur in an annotated gene (Figure 3A), namely PF15, which encodes the p80 subunit of katanin (Hartman *et al.*, 1998; McNally *et al.*, 2000; Dymek *et al.*, 2004), and we therefore chose this insertional line for further analysis. Genomic PCR revealed that the insertional mutagenic event deleted all but the first three predicted exons of the PF15 gene (Figure 3B). Mutations in the PF15 gene were previously identified in screens for paralyzed flagellar motility (Dymek *et al.*, 2004), and consistent with this result, we observed that in addition to its length defect, the mutant 1464 flagella were paralyzed. Because the original *pf15a* strain was previously shown to lack the central pair of microtubules (Adams *et al.*, 1981; Dymek *et al.*, 2004), we examined the structure of axonemes in mutant 1464 by electron microscopy (Figure 3C). For the wild type, 38 flagella were analyzed, all of which had a central pair. For the mutant 1464, 32 flagella were analyzed, of which 30 lacked a central pair and two contained electron-dense material in the center of the axoneme that could not be clearly recognized as a central pair. If these two are conservatively classified as positive, the fraction of flagella with a central pair is 100% for the wild type and 6% for the mutant. The central-pair defect seen in mutant 1464 is thus comparable to that seen in *pf15a* mutants.

We outcrossed mutant line 1464 containing the insertion in PF15 with wild-type cells and analyzed the genotype and phenotype of random progeny from 135 independent tetrads using a quadruple-redundant PCR strategy to identify the presence of the 1464 mutant–specific insertion in the PF15 gene and a visual screen for flagellar length and motility to identify the flagellar phenotype. No recombinants were identified that separated the insertion from the shf or paralyzed phenotypes, giving high confidence that the insertional event that we tracked was linked to the mutation causing the shf phenotype in line 1464.

However, the insertion in mutant 1464 was accompanied by deletion of several genes (Figure 3A), as judged by genomic PCR using primer pairs spanning the region. To determine whether mutation in the PF15 gene itself is sufficient to cause the length and pool regeneration defects seen in mutant 1464, we examined another independent allele of the PF15 gene, *pf15a* (Dymek *et al.*, 2004), to ask whether it shows the same length and pool regeneration phenotype. The *pf15a* strain contains a point mutation in the second exon of the PF15 gene, giving rise to a single amino acid substitution, V43D (Dymek *et al.*, 2004). We measured the flagellar length distribution in *pf15a* mutants and found that the *pf15a* strain exhibits heterogeneous flagellar lengths with a negative kurtosis, virtually identical to mutant 1464 (Figure 3D). We also found that *pf15a* mutant cells share the same slow regeneration kinetics (Figure 3E) and the same defect in regenerating the functional pool of flagellar precursors (Figure 3F) as in mutant 1464, and both mutant strains induce similar RSP3 expression (Figure 3G). The identical phenotypes of our insertional mutant and the *pf15a* point mutant indicate that PF15 mutation is indeed the cause of the *shf* phenotype. We designated our insertional allele of PF15 as *pf15-2*. The fact that the shf and pool regeneration phenotypes are virtually identical in two completely independent PF15 mutations indicates that katanin somehow plays a role in flagellar length and precursor pool mobilization.

To test for an effect of katanin p80 mutation on microtubule stability, we cultured cells on solid media containing either the microtubule-depolymerizing herbicide oryzalin (James *et al.*, 1993) or the microtubule-stabilizing compound Taxol. Neither the insertional mutant *pf15-2* nor the *pf15a* point mutant showed enhanced resistance or susceptibility to the antimicrotubule agents as compared with a wild-type strain, suggesting that the effect of the mutations on microtubule dynamics, if any, may be fairly subtle. It should be noted, however, that Taxol is less effective in most algae, including *Chlamydomonas*, than it is in animal cells, so a negative result for Taxol sensitivity is not informative.

Computational modeling of katanin activity in flagellar length control

It was previously shown that when flagella regenerate, cytoplasmic microtubules shorten transiently (Wang *et al.*, 2013), suggesting that cytoplasmic microtubules and flagella are competing for a common pool of tubulin. Because the *pf15* mutants in katanin show reduced mobilization of the precursor pool, we hypothesized that this slow mobilization might reflect the competition for a limited quantity of total tubulin between flagellar microtubules and cytoplasmic microtubules described by Wang *et al.* (2013) with katanin-mediated cleavage, making tubulin more available for flagellar growth. The *Chlamydomonas* cell contains two types of microtubules in the cytoplasm: four highly stable microtubule bundles known as rootlets (Ringo, 1967; Holmes and Dutcher, 1989) and ~10–20 nonroot microtubules (Schibler and Huang, 1991; Horst *et al.*, 1999). Because the rootlet microtubules are highly stable, we postulate that the nonroot microtubules contain a dynamic pool of tubulin and that growth of flagella competes with

short-flagella mutants. Graph shows expression of RSP3 (normalized by expression of RBCS2 housekeeping gene) vs. time after pH shock measured by quantitative PCR, comparing wild-type cells, *pf18* (chosen as a representative paralyzed mutation), and three previously described short-flagella mutants. Normal cells show up-regulation of flagella-specific genes at the 30- and 45-min time points, with expression dropping by 1 h. (F) Normalized expression of RSP3 in wild type and insertional short-flagella mutants. Error bars are SD among three separate experiments. Asterisks designate strains in which induction was significantly reduced ($p < 0.001$) compared with wild-type cells as determined by one-way analysis of variance, followed by Bonferroni's multiple comparison test.

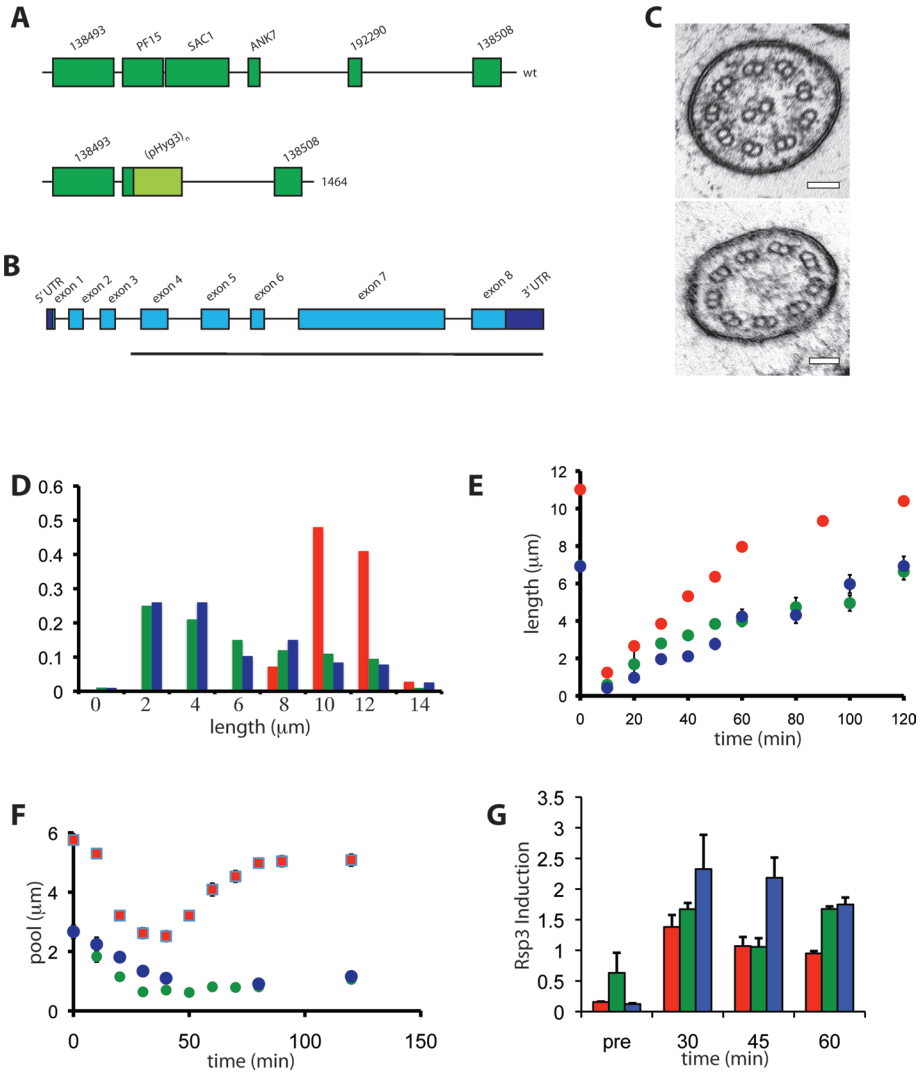

FIGURE 3: Mutation in p80 subunit of katanin results in short flagella with impaired precursor pool mobilization. (A) Position of pHyg insertion and accompanying deletion in genome of 1464 mutant as determined by RESDA mapping, followed by genomic PCR with flanking primers. (B) Region of PF15 gene that is deleted in the 1464 mutant, indicated by the solid bar below the gene map. (C) Electron microscopy showing loss of central pair microtubules in 1464 mutant. Top, wild-type cell showing clear central pair microtubules. Bottom, mutant 1464, showing that central-pair microtubules are missing and replaced with amorphous electron-dense material, similar to what is seen in the *pf15a* mutant. Scale bars, 50 nm. (D) Length distribution in wild type (red), mutant 1464 (green), and *pf15a* (blue). (E) Regeneration kinetics after pH shock in wild type (red), mutant 1464 (green), and *pf15a* (blue). Error bars show SE. (F) Comparison of effective pool regeneration kinetics for strain 1464 and *pf15a* measured by double-pH-shock procedure; red, wild type, green, 1464; blue, *pf15a*. (G) Comparison of flagellar gene induction in strain 1464 and *pf15a* measured by quantitative PCR. Plot shows ratio of RSP3 to RuBisCo message for wild type (red), 1464 (green), and *pf15a* (blue). Error bars show SD.

these microtubules for a shared tubulin pool. In this model, reduced katanin activity would lead to sequestration of tubulin by the cytoplasmic microtubules, causing shorter average flagellar length, as well as slower mobilization of the precursor tubulin pool during flagellar regeneration. To test whether this conceptual model could in principle explain the effects of the *pf15* mutants, we implemented a computational model that combines an ordinary differential equation model for flagellar length (Marshall and Rosenbaum, 2001) with a stochastic model for cytoplasmic microtubule dynamics (Gregoretti *et al.*, 2006). In this model, a single shared pool of tubulin is used for assembly of flagella and cytoplasmic microtubules (Figure 4A). We implemented a stochastic simulation of flagellar dynamics coupled to cytoplasmic microtubule dynamics. For this simulation, we implemented the model of microtubule dynamics described by Goodson and coworkers (Gregoretti *et al.*, 2006), in which each microtubule is represented as a linear polymer of subunits that can be either GTP or GDP bound. We recognize that such single-protofilament-type models do not capture the full richness of microtubule dynamics and that in the future, more realistic models should be applied (Bowne-Anderson *et al.*, 2013). Here we use this model simply to determine whether modulation of microtubules is at least in principle capable of affecting the apparent rate of flagellar precursor pool regeneration. At each time step, a decision is made to either release the final subunit, based on the GTP state of the penultimate subunit, or bind a new subunit based on the free tubulin concentration and the GTP state of the terminal subunit. The simulation of microtubules and the parameters of the model were based on those previously reported (Gregoretti *et al.*, 2006) and are given here as probability per unit time of a given event: probability of GTP hydrolysis, $K_{hydrolysis}$ = 0.1 s^{-1}; probability to add a subunit when the GTP cap is present, K_{grow_GTP} = 2.0 s^{-1}; probability to add a subunit when there is no GTP cap, K_{grow_GDP} = 0.10 s^{-1}; and probability to remove a subunit when there is no GTP cap, K_{shrink_GDP} = 48 s^{-1}. Following the approach of Gregoretti *et al.* (2006), we assume that shrinkage never occurs when the GTP cap is present. We note that for *Chlamydomonas*, none of the relevant kinetic parameters of microtubule dynamics has been reported; hence we use these parameters based on approximate values for mammalian cells discussed in Gregoretti *et al.* (2006). As was done by Gregoretti *et al.* (2006), we assume that regeneration of soluble GTP tubulin from disassembled GDP tubulin is instantaneous.

In our model, we simulated 10 cytoplasmic microtubules at once. The number of microtubules chosen for the simulation was based on three-dimensional microscopy images of *Chlamydomonas* cytoplasmic microtubules (Horst *et al.*, 1999). We did not implement a constraint on microtubule length because even though the cell has a finite diameter, its round shape allows microtubules to bend and wrap back around it when they become too long, as directly seen in certain *Chlamydomonas* mutants having unusually long microtubules (Horst *et al.*, 1999).

We augmented the existing microtubule dynamics model with a random cutting process to simulate katanin-mediated severing. At each time step, there was a constant probability of cutting a microtubule at any subunit. If a cut occurred, the site of the cut became the new final subunit, which maintained its GTP/GDP state before

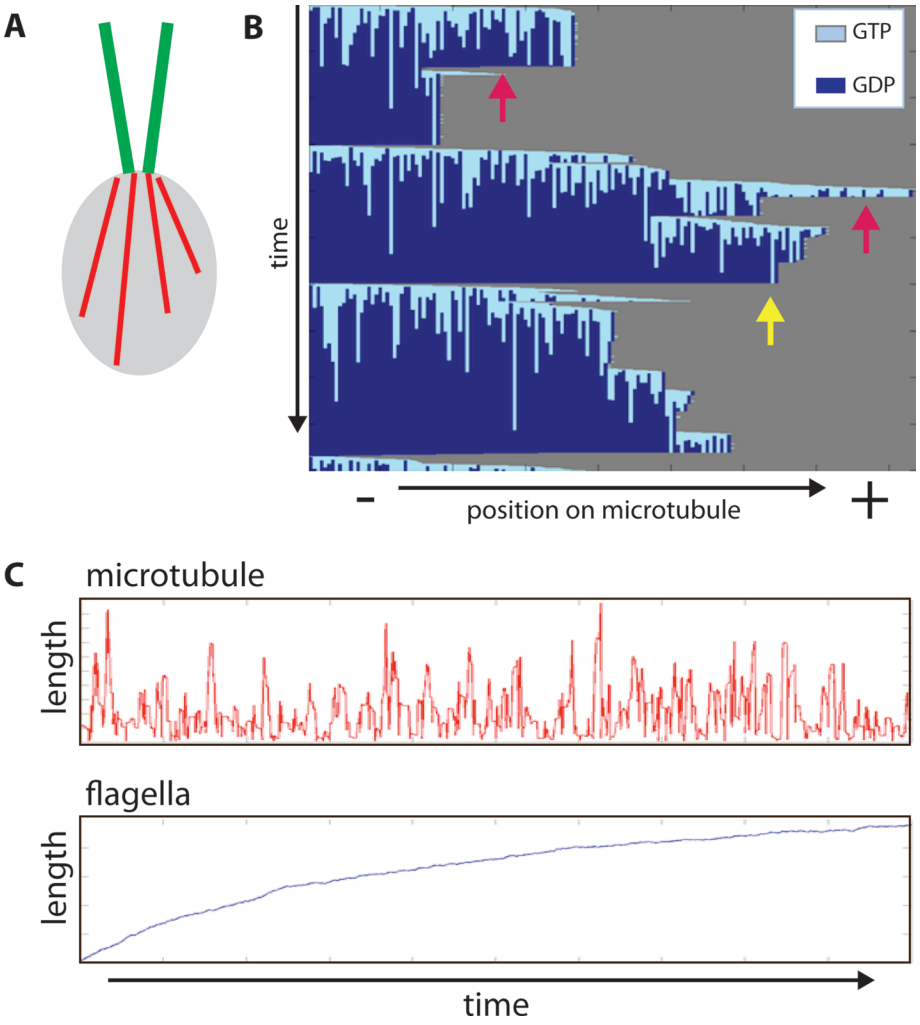

FIGURE 4: Combined model of flagellar and cytoplasmic microtubule dynamics. (A) Diagram illustrating two populations of microtubules; red, cytoplasmic microtubules; green, flagellar microtubules. (B) Kymograph showing a single run of stochastic microtubule simulation using the method of Gregoretti *et al.* (2006), with addition of katanin-mediated cleavage. The plot shows a single microtubule, with subunits color coded to indicate nucleotide state. Arrows indicate examples of katanin-mediated severing events (red arrows) and a catastrophe induced by spontaneous loss of GTP cap (yellow arrow). These events are distinguishable in the kymograph because catastrophe is preceded by loss of the GTP cap. We note that microtubules regrow more rapidly after catastrophe than after severing in the simulation because shrinkage after catastrophe ends when a full cap is restored, leading to immediate growth, whereas severing often produces a microtubule that lacks a cap and does not start growing until a full cap is assembled. (C) Example of simulation showing length fluctuations of one cytoplasmic microtubule in parallel with length changes in one flagellum as the flagellum grows from an initial zero length, thus representing a regeneration experiment. We note that these data are plotted on a longer time scale than in B, so that variation in flagellar length, which takes place much more slowly than variation in individual microtubules, can be observed.

the cut. The remaining subunits were then returned to the soluble pool. The combination of simulated microtubule spontaneous dynamics and katanin-mediated severing is illustrated in one example simulation in Figure 4B.

Flagellar growth dynamics was simultaneously simulated using an ordinary differential equation model previously described (Marshall and Rosenbaum, 2001), in which flagellar length changes according to the relation

$$\frac{dL_i}{dt} = \frac{AF}{L_i} - D \qquad (1)$$

where L_i is the length of the ith flagellum (normal *Chlamydomonas* cells have just two flagella, but we preserve the option to simulate mutants with altered flagellar number) and F is the quantity of free tubulin in the cytoplasm. Here D is the rate of flagellar microtubule disassembly, and A is a constant that describes the efficacy of intraflagellar transport.

In our simulations, we modeled two flagella but assume them to always have equal length; hence we have a single equation for flagellar length. We modified this equation to incorporate a first-order dependence of flagellar growth rate on free tubulin concentration. We augmented this equation with a single equation for the quantity of free tubulin dimer:

$$\frac{dL}{dt} = \frac{AvK[T_{free}]}{L} - D \qquad (2)$$

$$T_{free} = T_{total} - T_{polymer} - \frac{bnL}{s} \qquad (3)$$

where L is the flagellar length, D is the rate of disassembly from the tip (0.011 μm/s), n is the number of flagella (two for a typical cell), K is an affinity constant describing first-order binding of free tubulin to IFT particles, v is the velocity of IFT particles (strictly speaking, the harmonic mean of the anterograde and retrograde speeds), and A is a constant that combines the number of IFT particles and their effective cargo-carrying capacity (for our simulations, we used $A = 0.022$ and $K = 0.001$). The constant b indicates the ratio of the number of tubulin subunits per unit length of axoneme versus per unit length of cytoplasmic microtubule (~18), and s is the size in micrometers of a tubulin dimer within the microtubule lattice. We assume that disassembly occurs at a constant rate D, independent of flagellar length. This is a simplifying assumption based on the fact that flagellar shortening is length independent when IFT is inactivated (Marshall and Rosenbaum, 2001); however, recent studies demonstrated that the disassembly rate can be up-regulated when flagella become too long via a pathway regulated by the cnk2 kinase (Hilton *et al.*, 2013). Because our model addresses situations in which flagella are shorter than wild type, we assume that this cnk2-mediated pathway will not be activated, and therefore it is not included in the model. We note that this model does not take into account the nucleotide state of the tubulin dimers, a simplifying assumption that we make based on the fact that axonemal microtubules do not undergo spontaneous dynamics when isolated and instead seem to rely on enzymatic catalysis for turnover.

At all times, the total quantity T of tubulin in the cell, which is the sum of the flagellar tubulin content, the cytoplasmic microtubule content, and the soluble tubulin pool, is kept constant.

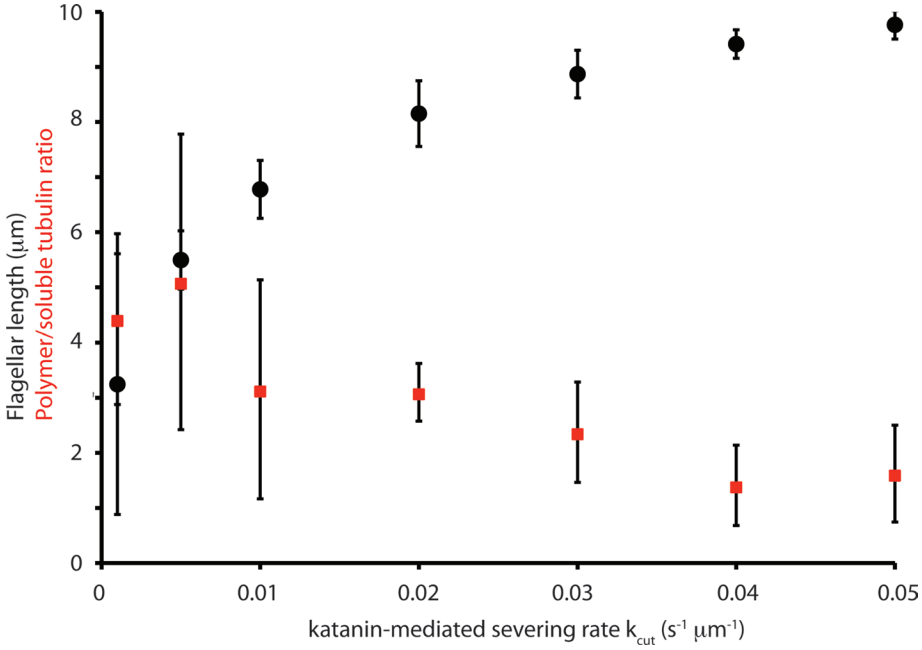

FIGURE 5: Predicted effect of changes in katanin-mediated microtubule severing on flagellar length. Flagellar length (black) and ratio of polymerized to soluble tubulin (red) are plotted for different values of the katanin severing rate parameter. Results show that as severing rate is decreased, flagellar length decreases. Polymerized/soluble ratio values are reported using the numerical values indicated on the *y*-axis.

To incorporate the effect of katanin activity, the probability of cutting an individual microtubule is assumed to be proportional to its length, such that for any given microtubule, the probability of it being cut in a given time step of the simulation is the product of the length, the size of the time step, and a rate constant, K_{cut}. Within the simulation, we represent mutations affecting katanin activity via changes in the value of K_{cut}. Using the foregoing parameters, a value for K_{cut} of 0.05 gave a steady-state flagellar length of ~10 μm.

We note that the model described here was deliberately intended to be as simple as possible. Simplifications include the assumption that severed portions of a microtubule are instantly depolymerized, the assumption that all soluble tubulin is in the GTP state, and the assumption of constant total tubulin.

With the combined model of cytoplasmic microtubule dynamics coupled with flagellar length dynamics in hand, we can simulate how both microtubule populations fluctuate in length over time in simulated regeneration experiments in which the flagellum is initialized at zero length and allowed to regenerate to a new steady-state length (Figure 4C). When many such simulations are combined, we find that decreasing the katanin-mediated severing of cytoplasmic microtubules produces a short steady-state flagellar length (Figure 5). With the particular parameters of this simulation, ~10-fold decrease in katanin activity would produce ~2-fold decrease in average flagellar length, similar to that seen in *pf15* mutants. Obviously, given the highly simplified nature of our model, it is not possible to directly infer the level of katanin activity change that would be necessary in a real cell, but the model does support the possibility that alteration in severing activity can in principle be sufficient to produce a change in flagellar length.

Modeling the role of kinesin-13 in flagellar length

It has been reported that depletion of a depolymerizing kinesin, kinesin-13, from *Chlamydomonas* leads to cells with regeneration defects and short flagella (Piao *et al.*, 2009; Wang *et al.*, 2013). Wang *et al.* (2013) proposed that these phenotypes could arise if kinesin-13 acts in the cytoplasm to help release tubulin from cytoplasmic microtubules for use in flagellar growth, a claim supported by the observation that cytoplasmic microtubules shorten less during flagellar regeneration when kinesin-13 is depleted by RNA interference (RNAi; Wang *et al.*, 2013). Because the proposed role for kinesin-13 in flagellar growth is similar to our model for katanin function, we modified the stochastic simulation of Figure 4 to simulate the effects of kinesin-13. This was done by adding a variable K_{remove}, which determines the probability per unit time of kinesin-13 removing the final tubulin from a microtubule (regardless of GTP state). We assume that the probability of terminal tubulin removal by kinesin-13 is independent of microtubule length, in contrast to the length-dependent activity of kinesin-8 (Varga *et al.*, 2006). With this additional term added to the model, we find that as the rate of kinesin-13 activity is increased, microtubules undergo higher frequency of catastrophe and gradually shorten during simulated flagellar regeneration (Figure 6A). When we plot steady-state flagellar length versus kinesin-13 activity (Figure 6B), we find that just as with katanin, increased activity leads to increased flagellar length. Decreased activity leads to short flagella. Our computational model thus recapitulates the key result of Wang *et al.* (2013) and further confirms that modulation of enzymes affecting cytoplasmic microtubule dynamics can alter flagellar length via a competition mechanism.

DISCUSSION

Relation to previous studies

Katanin has been shown to affect flagellar length in other organisms. Mutations in the p60 subunit of katanin cause short cilia length in *Tetrahymena* (Sharma *et al.*, 2007). The *Chlamydomonas* PF19 gene encodes one of the p60 catalytic subunits of katanin contained in the *Chlamydomonas* genome (Dymek and Smith, 2012). Our measurements of length distributions (Table 1) showed that the *pf19* mutant has a short average length and a broad length distribution comparable to *pf15* mutants. This result thus further supports the idea that katanin activity plays a role in determining flagellar length. We also note that prior studies showed that reduction of katanin function can cause increased microtubule polymer mass (Srayko *et al.*, 2006) and increased length of mitotic spindle microtubules (Goshima and Scholey, 2010; Loughlin *et al.*, 2011).

Analysis of the microtubule-depolymerizing kinesin, CrKinesin-13, of *Chlamydomonas* supports the idea that turnover of cytoplasmic microtubules facilitates availability of tubulin for flagellar growth. RNAi-mediated knockdown of the CrKinesin-13 gene caused a short-flagella phenotype similar to what we see in *pf15*, and these cells exhibit abnormally slow regeneration kinetics (Piao *et al.*, 2009). After deflagellation, CrKinesin-13 knockdown cells undergo a lag phase of ~1 h before beginning to regenerate their flagella, after which the flagella grow very slowly, reaching preshock length only after 4 h, suggesting that mobilization of the flagellar precursor pool is impaired. More recently, Pan and coworkers found that cytoplasmic

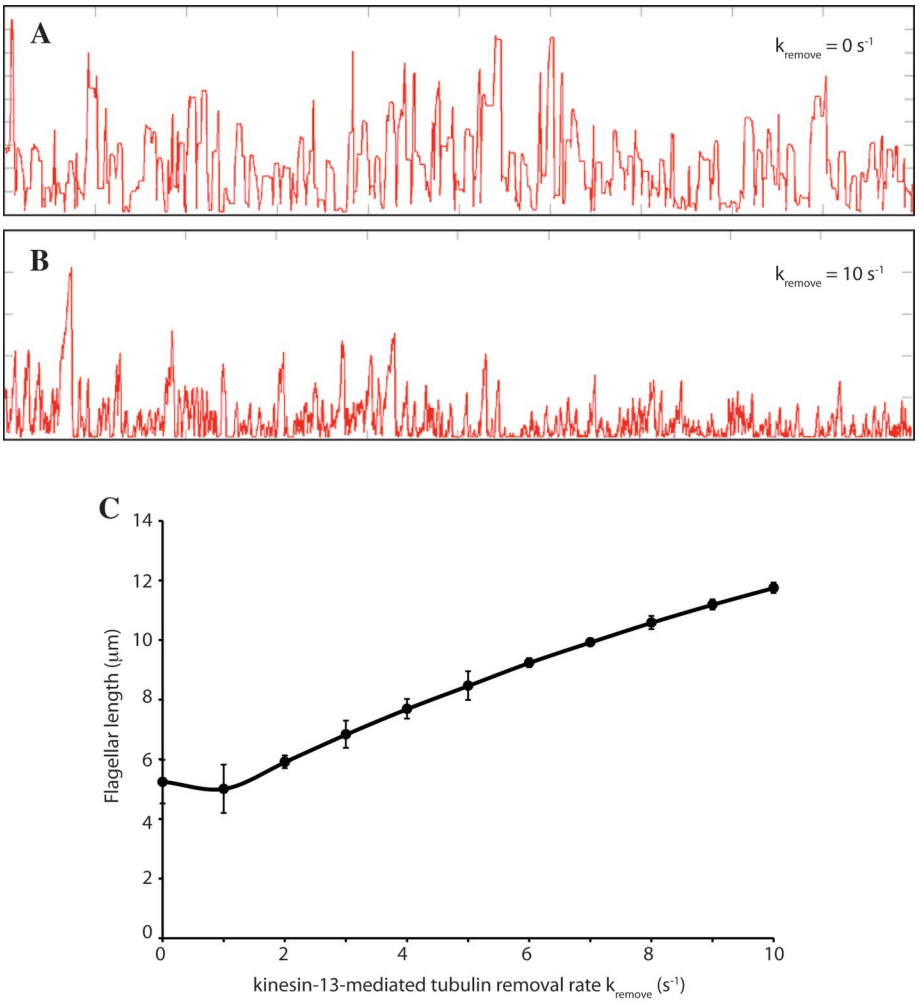

FIGURE 6: Modeling effect of kinesin-13–mediated microtubule shortening on flagellar length. (A) Microtubule length fluctuation during simulated flagellar regeneration in the absence of kinesin-13 activity. (B) Microtubule length fluctuation during flagellar regeneration in the presence of kinesin-13 activity, showing higher catastrophe frequency and gradual shortening of microtubules as flagella grow. (C) Steady-state flagellar length vs. simulated kinesin-13 activity.

microtubules depolymerize during flagellar regeneration and that this depolymerization is mediated in part by kinesin-13 (Wang *et al.*, 2013). They are thus able to explain the previous results of kinesin-13 RNAi by arguing that in the knockdown cells, cytoplasmic microtubules become more stable and thus compete more effectively for tubulin against flagellar microtubules. Our experimental and computational results suggest that a similar mechanism is likely to explain the short-flagella phenotype in *pf15* mutants.

A similar role has been discussed for proteins involved in actin filament turnover; for example, Aip1 promotes generation of actin monomers from partially disassembled actin filaments, thus providing an assembly-competent precursor pool to support assembly of other actin filaments (Okreglak and Drubin, 2010).

Studies in other protists indicate an opposite role of microtubule-severing or microtubule-depolymerizing proteins in flagellar length control. Mutations affecting microtubule-depolymerizing kinesins affect flagellar length in *Leishmania* (Blaineau *et al.*, 2007), but in that case, the effect is the opposite of what is seen in *Chlamydomonas*: depletion of kinesin-13 in *Leishmania* results in flagella that are longer, not shorter. Similarly, dominant negative alleles of kinesin-13 in *Giardia* cause flagella to become abnormally long (Dawson *et al.*, 2007). For katanin itself, overexpression in trypanosomes and *Leishmania* caused flagella to become shorter, not longer, again a result that seems to be the opposite of what we observe in *Chlamydomonas* (Cassanova *et al.*, 2009). The authors who reported these findings favor a type of model in which katanin or kinesin-13 functions primarily within the flagellum, and this could indicate a fundamental difference in flagellar length regulation between these organisms and *Chlamydomonas*.

Finally, we note that katanin has been shown to play a role in mitotic spindle length regulation (Loughlin *et al.*, 2011), but in that case it is believed that katanin is acting directly on the spindle microtubules themselves, such that a decrease in severing activity makes the spindle as a whole longer. Thus, although the spindle represents a clear case of katanin regulating the size of a microtubule-based structure, it is by an entirely different mechanism than the tubulin competition model we hypothesize for flagellar length regulation.

Role of precursor competition in organelle size determination

Our results with katanin, as well as published results with kinesin-13 in *Chlamydomonas* (Wang *et al.*, 2013), are consistent with the idea that within a single cell, there are differentially regulated sets of microtubules with differing functions, such as the stabilized microtubules of the flagellar axoneme and the more dynamic population in the cell body. In the biflagellate golden-brown alga *Ochromonas*, distinct sets of microtubules give rise to different aspects of the cell's characteristic pyriform shape (Brown and Bouck, 1973), and in this system it was clearly shown that as flagella grow, specific sets of cytoplasmic microtubules transiently shorten. Our model of competition between flagellar and cytoplasmic microtubules in *Chlamydomonas* thus has a precedent in *Ochromonas*. Consistent with the results in *Chlamydomonas* and *Ochromonas*, Sharma *et al.* (2011) showed that increasing the pool of soluble tubulin in mammalian cells with a carefully titrated dose of nocodazole correlates with longer cilia. Competition for precursor between different cytoskeletal structures has recently been reported for the actin cytoskeleton (Burke *et al.*, 2014). Taken together, these results argue that the size and assembly of individual cellular components cannot be treated in isolation and that the size of a particular cellular structure will depend at least in part on the competition between that structure and any other structures sharing common limiting pools of key components, much as the population sizes of distinct predators depend in part on the dynamics of shared prey populations.

MATERIALS AND METHODS

Strains and culture

C. reinhardtii cells were maintained on Tris-acetate-phosphate (TAP) plates (Harris, 1989), and experimental cultures were grown in M1

minimal medium (Harris, 1989). Insertional mutants were obtained in our lab in a previously reported screen (Feldman *et al.*, 2007), and additional strains were obtained from the *Chlamydomonas* Genetics Center (Duke University, Durham, NC). Cells were cultured at 21°C with constant light and in a rotating roller drum to provide aeration. Short-flagella (shf) reference alleles used in this study were *shf1*-253, *shf2*-1249, and *shf3*-1851.

Length measurements

Cells were fixed in 1% glutaraldehyde in phosphate-buffered saline (PBS) and imaged using differential interference contrast (DIC) optics with a 60× objective on a DeltaVision microscope. Measurements were obtained by hand tracing flagella using Softworx software. Only cells with two visible, measurable flagella were included in the analysis.

Analysis of length distributions

Length measurement data were analyzed using Excel (Microsoft) to calculate skew and excess kurtosis values (Taylor, 1996). Skew was determined to be significant if the skew value was greater than twice the SE of skew, defined as $\sqrt{6/N}$. Kurtosis was determined to be significant if the excess kurtosis value was greater than twice the SE of kurtosis, defined as $\sqrt{24/N}$.

Deflagellation by pH shock

Cells were spun down at 1500 × *g* for 2 min in a bench-top centrifuge and resuspended in M1 medium acidified to pH 4.5 with acetic acid. After a 1-min incubation in acidic M1, medium was returned to neutral pH by addition of KOH, cells were centrifuged again, supernatant was decanted, and cells were resuspended in fresh neutral M1 medium.

Flagellar regeneration assay

Cells were subjected to acidic pH shock as described. Resuspended cells in neutral M1 medium were incubated at 21°C with constant light in a rotating roller drum. Aliquots of cells were withdrawn at 10-min intervals and mixed with an equal volume of 2% glutaraldehyde in 1× PBS to fix. Length measurements were performed as described.

Quantitative reverse transcription PCR

To measure gene expression during flagellar assembly, total RNA was isolated from *Chlamydomonas* cells before deflagellation and at 30, 45, and 60 min after deflagellation as previously described (Stolc *et al.*, 2005), with an additional purification step using a PureLink RNA minikit (Life Technologies, Grand Island, NY). RNA was reverse transcribed using the SuperScript VILO kit (Life Technologies), with 1 μg of total RNA per reaction. cDNA was diluted 1:20 and used for quantitative PCR with Taq and SYBR Green and analyzed with a DNA Engine Opticon system (MJ Research, St. Bruno, Quebec, Canada). C_T values were obtained using Opticon software (MJ Research).

Flagellar precursor pool estimation

Cells were subjected to deflagellation by pH shock as described. At 10-min intervals after the initial shock, cells were subjected to a second shock with cycloheximide at 10 μg/ml final concentration in both the acidic shock medium and neutral recovery medium. Cells were permitted to recover from the second shock for 2 h before fixation, and flagellar length measurements were performed as described.

Isolation of genomic DNA

Two procedures were used for isolation of genomic DNA: a dual extraction process for harvesting clean genomic DNA for sensitive downstream applications such as RESDA-PCR, and a rapid, crude preparation for genotyping PCR. Clean genomic DNA was obtained using a CTAB/chloroform extraction protocol, followed by a second extraction with phenol chloroform. Cells were grown in TAP medium with shaking under continuous light and harvested by centrifugation. Cells were then frozen at −80°C and lyophilized overnight. Lysis was achieved by vortexing with glass beads in CTAB extraction buffer (100 mM Tris-HCl, pH 7.5, 0.7 M NaCl, 10 mM EDTA, 1% cetyltrimethyl ammonium bromide [CTAB], 1% β-mercaptoethanol), followed by incubation at 65°C for 2 h. Subsequent chloroform extraction, isopropanol precipitation, phenol chloroform extraction, and ethanol precipitation were performed using standard methods. The resulting DNA was treated with 50 μg/ml RNase A at 37°C for 1 h and 0.5 mg of proteinase K at 55°C for 1 h. Crude DNA was prepared using a modified smash-and-grab protocol for *Saccharomyces cerevisiae*.

Identification of flanking sequence

RESDA-PCR was performed as described in Gonzalez-Ballester *et al.* (2005) using the following primers specific for the mutagenizing plasmid:

HYG 5′ R7 TTGCCGGGAAGCTAGAGTAAG
HYG 5′ R9 GCCATCCGTAAGATGCTTTTC
HYG 5′ R6 ATACGGGAGGGCTTACCATCT
HYG 3′ F6 CAGAGGTTTTCACCGTCATCA
HYG 3′ F8 CGAGTGGGTTACATCGAACTG
HYG 3′ F5 GCTGCATGTGTCAGAGGTTTT
HYG 3′ F7 TTTTGCCTTCCTGTTTTTGCT

Nested PCR products were subjected to gel electrophoresis, followed by excision of discrete bands. PCR products were isolated using a gel purification kit (Qiagen, Valencia, CA), cloned using a TOPO-TA cloning system (Life Technologies), and sequenced. Identified sequence was compared with the *Chlamydomonas* genome, version 3.0.

Genotyping PCR

Primer pairs were designed such that products specific for the presence or absence of the insertion identified in mutant 1464, located in genomic scaffold 34, would be amplified:

1464 insert+ F1 GACACCAGTCGTCGGTGGAGAGTGT
1464 insert+ R1 TCCGTGTCGCCCTTATTCCCTTTTT
1464 insert– F1 AGCTTTGTAAGTGGAGGGGGCAACC
1464 insert– R1 GAGGTGTATGGGGTTGTTGCCGAGT

Motility phenotype assessment

After 2 d in liquid culture, aliquots of live cells were subjected to DIC microscopy using a 20× objective, and swimming behavior was assessed visually.

Electron microscopy

Exponentially growing wild-type and PF15 mutant *Chlamydomonas* were collected by filtration and processed as described (Schuck *et al.*, 2009). In brief, cells were frozen using a Leica (Wetzlar, Germany) EM PACT high-pressure freezer, fixed with 1% osmium tetroxide, 0.1% uranyl acetate, and 3% water in acetone using a Leica EM AFS2 freeze substitution machine, and embedded in Epon resin. Sections 40 nm in thickness were cut, stained with 2% aqueous uranyl acetate and Reynold's lead citrate, and viewed under a

FEI (Hillsboro, OR) Tecnai T12 electron microscope. To quantify the fraction of flagella with a central pair, micrographs were acquired of flagella cross-sectioned such that all nine outer doublet microtubules were visible, and the presence of a discernible central pair was scored.

Microtubule drug resistance assay

TAP agar was prepared and autoclaved as described previously (Harris, 1989). Before pouring plates, the desired drug was added to the medium (oryzalin at final concentrations of 2, 20, and 40 μM). Cells were streaked onto cooled plates and incubated in constant light for 1 wk before growth was assessed visually.

Stochastic simulation of competition for tubulin

The equations were solved using the Euler method with a time step of 0.02 s, and at each time step, the free tubulin pool size T_{free} was updated based on the stochastic microtubule dynamics simulation running in parallel. We deliberately chose a time step small enough that the probability of more than one microtubule dynamics event (catastrophe, rescue, or cutting) was negligible.

We simulate stochastic cutting by katanin by generating a uniformly distributed random number and comparing it to the probability of cutting a given microtubule during any single time step. Once the decision is made to cut a microtubule, the position of the cut is chosen at random from a uniform distribution of positions spanning the full length of the microtubule. All tubulin subunits contained in the cut portion are returned to the free pool and set to the GTP-bound state. The fact that this occurs instantaneously is a simplification of the model.

ACKNOWLEDGMENTS

We thank Peter Walter for support and Holly Goodson for helpful advice. This work was funded by National Institutes of Health Grant R01 GM097017.

REFERENCES

Adams GM, Huang B, Piperno G, Luck DJ (1981). Central-pair microtubular complex of Chlamydomonas flagella: polypeptide composition as revealed by analysis of mutants. J Cell Biol 91, 69–76.

Asleson CM, Lefebvre PA (1998). Genetic analysis of flagellar length control in Chlamydomonas reinhardtii: a new long-flagella locus and extragenic suppressor mutations. Genetics 148, 693–702.

Barsel SE, Wexler DE, Lefebvre PA (1988). Genetic analysis of long-flagella mutants of Chlamydomonas reinhardtii. Genetics 118, 637–648.

Bhogaraju S, Cajanek L, Fort C, Blisnick T, Weber K, Taschner M, Mizuno N, Lamla S, Bastin P, Nigg EA, *et al.* (2013). Molecular basis of tubulin transport within the cilium by IFT74 and IFT81. Science 341, 1009–1012.

Blaineau C, Tessier M, Dubessay P, Tasse L, Crobu L, Pages M, Bastien P (2007). A novel microtubule-depolymerizing kinesin involved in length control of a eukaryotic flagellum. Curr Biol 17, 778–782.

Bowne-Anderson H, Zanic M, Kauer M, Howard J (2013). Microtubule dynamic instability: a new model with coupled GTP hydrolysis and multistep catastrophe. Bioessays 35, 452–461.

Brown DL, Bouck GB (1973). Microtubule biogenesis and cell shape in Ochromonas. II. The role of nucleating sites in shape development. J Cell Biol 56, 360–378.

Burke TA, Christensen JR, Barone E, Suarez C, Sirotkin V, Kovar DR (2014). Homeostatic actin cytoskeleton networks are regulated by assembly factor competition for monomers. Curr Biol 24, 579–585.

Cassanova M, Crobu L, Blaineau C, Bourgeois N, Bastien P, Pages M (2009). Microtubule-severing proteins are involved in flagellar length control and mitosis in trypanosomatids. Mol Microbiol 71, 1353–1370.

Chan YH, Marshall WF (2010). Scaling properties of cell and organelle size. Organogenesis 6, 88–96.

Dawson SC, Sagolla MS, Mancuso JJ, Woessner DJ, House SA, Fritz-Laylin L, Cande WZ (2007). Kinesin-13 regulates flagellar, interphase, and mitotic microtubule dynamics in Giardia intestinalis. Eukaryotic Cell 6, 2354–2364.

Decker M, Jaensch S, Pozniakovsky A, Zinke A, O'Connell KF, Zachariae W, Myers E, Hyman AA (2011). Limiting amounts of centrosome material set centrosome size in C. elegans embryos. Curr Biol 21, 1259–1267.

Dymek EE, Lefebvre PA, Smith EF (2004). PF15p is the Chlamydomonas homologue of the Katanin p80 subunit and is required for assembly of flagellar central microtubules. Eukaryot Cell 3, 870–879.

Dymek EE, Smith EF (2012). PF19 encodes the p60 catalytic subunit of katanin and is required for assembly of the flagellar central apparatus in Chlamydomonas. J Cell Sci 125, 3357–3366.

Engel BD, Ludington WB, Marshall WF (2009). Intraflagellar transport particle size scales inversely with flagellar length: revisiting the balance-point length control model. J Cell Biol 187, 81–89.

Feldman JL, Geimer S, Marshall WF (2007). The mother centriole plays an instructive role in defining cell geometry. PLoS Biol 5, e149.

Goehring NW, Hyman AA (2012). Organelle growth control through limiting pools of cytoplasmic components. Curr Biol 22, R330–R339.

Gonzalez-Ballester D, Montaigu A de, Galvan A, Fernandez E (2005). Restriction enzyme site-directed amplification PCR: a tool to identify regions flanking a marker DNA. Anal Biochem 340, 330–335.

Goshima G, Scholey JM (2010). Control of mitotic spindle length. Annu Rev Cell Dev Biol 26, 21–57.

Gregoretti IV, Margolin G, Alber MS, Goodson HV (2006). Insights into cytoskeletal behavior from computational modeling of dynamic microtubules in a cell-like environment. J Cell Sci 119, 4781–4788.

Hao L, Thein M, Brust-Mascher I, Civelekoglu-Scholey G, Lu Y, Acar S, Prevo B, Shaham S, Scholey JM (2011). Intraflagellar transport delivers tubulin isotypes to sensory cilium middle and distal segments. Nat Cell Biol 13, 790–798.

Harris EH (1989). The Chlamydomonas Sourcebook : A Comprehensive Guide to Biology and Laboratory Use, San Diego, CA: Academic Press.

Hartman JJ, Mahr J, McNally K, Okawa K, Iwamatsu A, Thomas S, Cheesman S, Heuser J, Vale RD, McNally FJ (1998). Katanin, a microtubule-severing protein, is a novel AAA ATPase that targets to the centrosome using a WD40-containing subunit. Cell 93, 277–287.

Hilton LK, Gunawardane K, Kim JW, Schwartz MC, Quarmby LM (2013). The kinases LF4 and CNK2 control ciliary length by feedback regulation of assembly and disassembly rates. Curr Biol 23, 2208–2214.

Holmes JA, Dutcher SK (1989). Cellular asymmetry in Chlamydomonas reinhardtii. J Cell Sci 94, 273–285.

Horst CJ, Fishkind DJ, Pazour GJ, Witman GB (1999). An insertional mutant of Chlamydomonas reinhardtii with defective microtubule positioning. Cell Motil Cytoskeleton 44, 143–154.

James SW, Silflow CD, Stroom P, Lefebvre PA (1993). A mutation in the alpha 1-tubulin gene of Chlamydomonas reinhardtii confers resistance to anti-microtubule herbicides. J Cell Sci 106, 209–218.

Keller LR, Schloss JA, Silflow CD, Rosenbaum JL (1984). Transcription of alpha- and beta-tubulin genes in vitro in isolated Chlamydomonas reinhardtii nuclei. J Cell Biol 98, 1138–1143.

Koroyasu S, Yamazato M, Hirano T, Aizawa SI (1998). Kinetic analysis of the growth rate of the flagellar hook in Salmonella typhimurium by the population balance method. Biophys J 74, 436–443.

Kuchka MR, Jarvik JW (1982). Analysis of flagellar size control using a mutant of Chlamydomonas reinhardtii with a variable number of flagella. J Cell Biol 92, 170–5.

Kuchka MR, Jarvik JW (1987). Short-flagella mutants of Chlamydomonas reinhardtii. Genetics 115, 685–691.

Lefebvre PA, Nordstrom SA, Moulder JE, Rosenbaum JL (1978). Flagellar elongation and shortening in Chlamydomonas. IV. Effects of flagellar detachment, regeneration, and resorption on the induction of flagellar protein synthesis. J Cell Biol 78, 8–27.

Lefebvre PA, Rosenbaum JL (1986). Regulation of the synthesis and assembly of ciliary and flagellar proteins during regeneration. Annu Rev Cell Biol 2, 517–546.

Levy DL, Heald R (2012). Mechanisms of intracellular scaling. Annu Rev Cell Dev Biol 28, 113–135.

Loughlin R, Wilbur JD, McNally FJ, Nedelec FJ, Heald R (2011). Katanin contributes to interspecies spindle length scaling in Xenopus. Cell 147, 1397–1407.

Ludington WB, Wemmer KA, Lechtreck KF, Witman GB, Marshall WF (2013). Avalanche-like behavior in ciliary import. Proc Natl Acad Sci USA 110, 3925–3930.

Marshall WF, Qin H, Rodrigo-Brenni M, Rosenbaum JL (2005). Flagellar length control system: testing a simple model based on intraflagellar transport and turnover. Mol Biol Cell 16, 270–278.

Marshall WF, Rosenbaum JL (2001). Intraflagellar transport balances continuous turnover of outer doublet microtubules: implications for flagellar length control. J Cell Biol 155, 405–414.
McNally KP, Bazirgan OA, McNally FJ (2000). Two domains of p80 katanin regulate microtubule severing and spindle pole targeting by p60 katanin. J Cell Sci 113, 1623–1633.
McVittie A (1972). Flagellum mutants of Chlamydomonas reinhardii. J Gen Microbiol 71, 525–540.
Okreglak V, Drubin DG (2010). Loss of Aip1 reveals a role in maintaining the actin monomer pool and an in vivo oligomer assembly pathway. J Cell Biol 188, 769–777.
Piao T, Luo M, Wang L, Guo Y, Li D, Li P, Snell WJ, Pan J (2009). A microtubule depolymerizing kinesin functions during both flagellar disassembly and flagellar assembly in Chlamydomonas. Proc Natl Acad Sci USA 106, 4713–4718.
Qin H, Diener DR, Geimer S, Cole DG, Rosenbaum JL (2004). Intraflagellar transport (IFT) cargo: IFT transports flagellar precursors to the tip and turnover products to the cell body. J Cell Biol 164, 255–266.
Ringo DL (1967). Flagellar motion and fine structure of the flagellar apparatus in Chlamydomonas. J Cell Biol 33, 543–571.
Rosenbaum JL, Moulder JE, Ringo DL (1969). Flagellar elongation and shortening in Chlamydomonas. The use of cycloheximide and colchicine to study the synthesis and assembly of flagellar proteins. J Cell Biol 41, 600–619.
Schibler MJ, Huang B (1991). The colR4 and colR15 beta-tubulin mutations in Chlamydomonas reinhardtii confer altered sensitivities to microtubule inhibitors and herbicides by enhancing microtubule stability. J Cell Biol 113, 605–614.
Schuck S, Prinz WA, Thorn KS, Voss C, Walter P (2009). Membrane expansion alleviates endoplasmic reticulum stress independently of the unfolded protein response. J Cell Biol 187, 525–536.
Sharma N, Bryant J, Wloga D, Donaldson R, Davis RC, Jerka-Dziadosz M, Gaertig J (2007). Katanin regulates dynamics of microtubules and biogenesis of motile cilia. J Cell Biol 178, 1065–1079.
Sharma N, Kosan ZA, Stallworth JE, Berbari NF, Yoder BK (2011). Soluble levels of cytosolic tubulin regulate ciliary length control. Mol Biol Cell 22, 806–816.
Srayko M, O'Toole ET, Hyman AA, Muller-Reichert T (2006). Katanin disrupts the microtubule lattice and increases polymer number in C. elegans meiosis. Curr Biol 16, 1944–1949.
Stolc V, Samanta MP, Tongprasit W, Marshall WF (2005). Genome-wide transcriptional analysis of flagellar regeneration in Chlamydomonas reinhardtii identifies orthologs of ciliary disease genes. Proc Natl Acad Sci USA 102, 3703–3707.
Taylor JR (1996). An Introduction to Error Analysis: The Study of Uncertainties in Physical Measurements, Sausalito, CA: University Science Books.
Varga V, Helenius J, Tanaka K, Hyman AA, Tanaka TU, Howard J (2006). Yeast kinesin-8 depolymerizes microtubules in a length-dependent manner. Nat Cell Biol 8, 957–962.
Wang L, Paio T, Cao M, Qin T, Huang L, Deng H, Mao T, Pan J (2013). Flagellar regeneration requires cytoplasmic microtubule depolymerization and kinesin-13. J Cell Sci 126, 1531–1540.
Wemmer KA, Marshall WF (2007). Flagellar length control in Chlamydomonas—a paradigm for organelle size regulation. Int Rev Cytol 260, 175–212.
Wilson NF, Iyer JK, Buchheim JA, Meek W (2008). Regulation of flagellar length in Chlamydomonas. Semin Cell Devel Biol 19, 494–501.
Wren KN, Craft JM, Tritschler D, Schauer A, Patel DK, Smith EF, Porter ME, Kner P, Lechtreck KF (2013). A differential cargo-loading model of ciliary length regulation by IFT. Curr Biol 23, 2463–2471.